Optical recognition of structural and electronic transformation of Pb ultrathin films

2004 J. Phys.: Condens. Matter 16 S4345

(http://iopscience.iop.org/0953-8984/16/39/009)

INSTITUTE OF PHYSICS PUBLISHING JOURNAL OF PHYSICS: CONDENSED MATTER

J. Phys.: Condens. Matter **16** (2004) S4345–S4352 PII: S0953-8984(04)78878-5

Optical recognition of structural and electronic transformation of Pb ultrathin films

M Jałochowski[1], **M Strożak and R Zdyb**

Institute of Physics, Maria Curie–Skłodowska University, Plac M Curie–Skłodowskiej 1, PL-20031 Lublin, Poland

E-mail: ifmkj@tytan.umcs.lublin.pl

Received 31 March 2004
Published 17 September 2004
Online at stacks.iop.org/JPhysCM/16/S4345
doi:10.1088/0953-8984/16/39/009

Abstract

In this study, the transformation of ultrathin Pb film on a Si(111)-(7 × 7) surface from amorphous-like to crystalline state is examined at low temperatures during the film growth by measuring the differential reflectance (DR) $\Delta R/R$, as a function of film thickness. The experiments were performed under ultrahigh vacuum conditions in the visible and infrared spectral range. The determined imaginary part of the Pb dielectric function changes steeply at the critical thickness of the film of about 5 monoatomic Pb(111) layers. High energy electron diffraction (RHEED) and scanning tunnelling microscopy (STM) studies revealed a film with fine granular morphology before the structural transition and a well ordered epitaxial layer after the transformation. The variation of the optical (AC) conductivity was compared with DC electrical conductance data. We show that the DR technique can be efficiently used to characterize structural and electronic changes in ultrathin metallic films.

1. Introduction

Several experimental studies have shown that Pb growing on Si(111) forms during the initial stage of the growth an amorphous-like layer [1, 2], which at a critical thickness undergoes a structural transition into a well defined crystalline and epitaxial layer [3]. This thickness varies with the temperature of the substrate from 7 ML at 18 K to 4 ML at 70 K [4]. The crystalline phase of the ultrathin Pb has been widely studied, mainly due to the presence of clear quantum size effects (QSE) [5–7]. Much less attention has been paid to the amorphous phase formed during initial stage Pb growth on cooled Si(111)-(7 × 7) substrates. Although x-ray investigations have confirmed a structural transition [8], little is known about the morphology and electronic properties of the Pb ultrathin film below the critical thickness. The knowledge of the structural and the electronic properties may help to understand the expected weak

[1] Author to whom any correspondence should be addressed.

localization [9] and insulator-to-metal transition [10] recently studied in the low-temperature quenched amorphous phase of the thin Pb film.

In this study we present detailed differential reflectivity (DR) measurements of the early stages of formation of the Pb ultrathin film on Si(111) substrate at temperatures as low as 105 K. The optical data are enhanced by scanning tunnelling microscopy (STM) and diffraction high energy electron diffraction (RHEED) data. The optical constant derived from the optical measurements is compared with the results of the electrical resistivity measurements of the ultrathin Pb films.

2. Experimental details

Samples were prepared in a UHV chamber equipped with an RHEED apparatus, and a gas-flow UHV liquid helium cryostat for cooling of the samples during film deposition and during optical measurements. The base pressure was 5×10^{-11} mbar. The Si samples with the dimensions of $18 \times 5 \times 0.6$ mm^3 and with 20 Ω cm specific resistivity at room temperature used here were fabricated from a p-type boron-doped single-crystal. Flashing for a few seconds to about 1500 K resulted in the removal of SiC and in the appearance of the (7×7) superstructure RHEED pattern. A direct resistive heating was used.

The differential reflectance (DR) technique consists of measurements of the relative change of a substrate reflectance upon thin film deposition: $\Delta R/R = (R^{\mathrm{Si+Pb}} - R^{\mathrm{Si}})/R^{\mathrm{Si}}$, where R^{Si} and $R^{\mathrm{Si+Pb}}$ are the reflectance of a bare substrate and a substrate covered by a Pb deposit, respectively. The angle of incidence of the light beam ϕ was equal to 47°. The apparatus consisted of a quartz halogen lamp, a prism monochromator, polarizer, a PbSe photoconductor for light energies below 1.2 eV and a Si-photodiode above this energy. The temperature of the detectors was stabilized at −10 °C. The light beam was chopped with frequency equal to 73 Hz. A lock-in technique was employed to recover the signal. s-polarized or p-polarized light entered the UHV chamber through a fused silica window and was focused on a sample. Convergence of the light beam at the sample was below 0.7°. The specularly reflected beam after passing a second fused silica window was focused on the detector. The intensity of the reflected light was recorded during the thin film deposition. The rate of Pb deposition was about 1 monoatomic layer of Pb(111) (ML) per min. Typically about 500 points of data were collected for each sample, with the final thickness of about 7 nm. During the deposition of Pb the substrate was held at 105 K. The crystal structure of the growing film was monitored with RHEED. Specularly reflected electron beam RHEED intensity oscillations were recorded simultaneously during optical reflectivity measurements and were used for the calibration of the quartz crystal thickness monitor.

The DC electrical conductivity experiment was made in the same UHV system, during the film deposition at low temperature, by passing a low frequency current and measuring the voltage drop along the sample. As voltage contacts sharp tungsten wires pressed against the Si(111)-(7×7) substrate were used [3]. This method allowed us to measure the electrical conductivity simultaneously with the DR measurements.

The samples studied with the STM were prepared in similar conditions in another UHV system equipped with an Omicron VT STM. Before being installed in the STM stage, the Si(111) substrates were carefully cleaned by flashing up to 1500 K. Next, in order to produce a large domain of homogeneous areas of reconstructed surface, the substrates were slowly cooled down during the $(1 \times 1) \longleftrightarrow (7 \times 7)$ transition. This process was controlled by the RHEED. Pb films of various thickness were deposited on such prepared substrates mounted in the cooled STM stage. The pressure of the chamber during the Pb deposition was below 7×10^{-11} mbar.

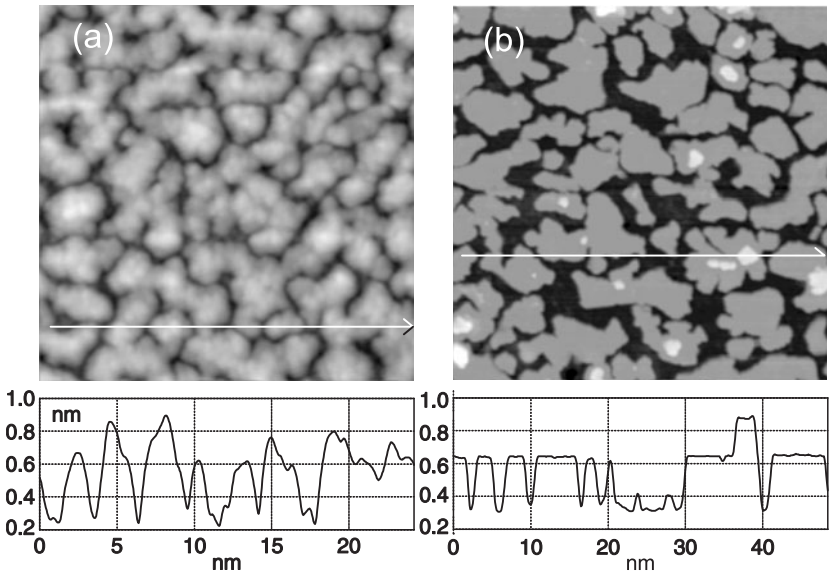

Figure 1. (a) 25 nm × 25 nm and (b) 50 nm × 50 nm STM topographic images and corresponding profiles for Pb on Si(111)-(7 × 7) substrate deposited at 105 K. In (a) the average coverage is equal to 3 ML. The sample is composed of irregular granular species separated by deep grooves. In (b) the average coverage is equal to 6.6 ML. The profile shows the well developed layered structure of the film.

3. Results and discussion

3.1. Structure of Pb film on Si(111)-(7 × 7) *substrate*

Figures 1(a), and (b) show STM topographic images of Pb films after deposition of 3, and 6.6 ML of Pb(111), respectively. Each figure is accompanied by a corresponding profile line. Figure 1(a) was recorded before the structural transition and figure 1(b) shortly after completion of the transition. These figures show a dramatic variation of the morphology with increasing coverage. The 3 ML thick sample is composed of a granular species with average size of about 2–3 nm. Their shape is irregular and the surface is rough. The granules are separated by deep grooves. The STM image shows that an individual granule has an internal fine structure and is composed of small grains with size of around 1 nm. The image shows clearly that at this thickness the Pb is highly disordered and does not form a crystalline structure.

The morphology of the thicker film, (figure 1(b)), differs dramatically from that displayed in figure 1(a). Here the film is composed of perfectly flat areas which we can identify with ordered layers of Pb(111). Three layers are visible: 5, 6 ML, and a small fraction of the seventh ML. The islands, still irregular, appear homogeneous. Although the STM data show unambiguously that the structural transformation involves surface atoms, it has been proved using surface x-ray diffraction [8], that this transformation also involves rearrangement of volume atoms.

The structural transition was observed *in situ*, using an RHEED diffraction technique. Figure 2 shows the RHEED electron specular beam intensity as a function of the average Pb thickness deposited on the substrate held at 105 K. Up to about 5 ML of Pb the RHEED intensity oscillates irregularly and is strongly damped. At the critical thickness of about 5 ML a new set of oscillations emerges. Now the period of oscillations corresponds exactly to 1 ML

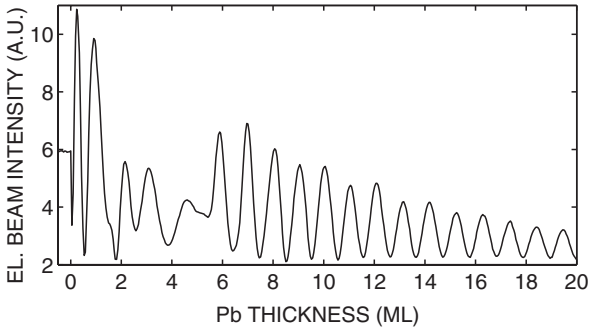

Figure 2. An example of RHEED intensity variation recorded during Pb deposition on Si(111)-(7 × 7) substrate at 105 K. The first diffraction streaks originating from the Pb crystalline phase appear at a thickness close to 5 ML, where RHEED oscillation recovers.

of Pb(111) and the damping is much weaker. This is sign of a layer-by-layer growth possible only in the well ordered crystalline phase. For a thickness smaller than 5 ML the RHEED pattern showed diffuse and concentric features, characteristic of randomly oriented and very small grains. The first diffraction streaks originating from the Pb(111) epitaxial layer appeared after deposition of about 5 ML Pb.

3.2. Differential reflectivity

The basic theory of the differential reflectivity of a system composed of a thin isotropic or anisotropic layer on a substrate has been well established for various physical situations [12–16]. The DR for an isotropic system [11], when the thickness of film d is small with respect to the wavelength λ of the incident light then for p-polarization is

$$\frac{R_{\mathrm{p}}^{\mathrm{Si+Pb}} - R_{\mathrm{p}}^{\mathrm{Si}}}{R_{\mathrm{p}}^{\mathrm{Si}}} = \frac{8\pi d}{\lambda} \cos\phi \,\mathrm{Im}\left\{ \frac{\varepsilon^{\mathrm{Pb}} - \varepsilon^{\mathrm{Si}}}{\varepsilon^{\mathrm{Si}} - 1} \frac{1 - \frac{\varepsilon^{\mathrm{Pb}} + \varepsilon^{\mathrm{Si}}}{\varepsilon^{\mathrm{Pb}}\varepsilon^{\mathrm{Si}}} \sin^2\phi}{1 - \frac{1+\varepsilon^{\mathrm{Si}}}{\varepsilon^{\mathrm{Si}}} \sin^2\phi} \right\}, \tag{1}$$

with $\varepsilon^{\mathrm{Pb}}$ and $\varepsilon^{\mathrm{Si}}$ being the complex dielectric function of Pb and Si, respectively. The expression (1) depends very weakly on the real part of the thin film dielectric function. For s-polarization the DR is

$$\frac{R_{\mathrm{s}}^{\mathrm{Si+Pb}} - R_{\mathrm{s}}^{\mathrm{Si}}}{R_{\mathrm{s}}^{\mathrm{Si}}} = \frac{8\pi d}{\lambda} \cos\phi \,\mathrm{Im}\left\{ \frac{\varepsilon^{\mathrm{Pb}} - \varepsilon^{\mathrm{Si}}}{\varepsilon^{\mathrm{Si}} - 1} \right\}. \tag{2}$$

The expression (2) is independent of the real part of the thin film dielectric function. For the geometry used in this work the $(R^{\mathrm{Si+Pb}} - R^{\mathrm{Si}})/R^{\mathrm{Si}}$ signal for p-polarization was about 2.5 times larger than for s-polarization. Therefore, in the following, only the results for p-polarization are discussed. We notice that dielectric functions calculated from p-polarization and s-polarization data were the same to within an accuracy of ±5% for all thicknesses.

The experimental data of the DR for p-polarization recorded during the film deposition, as a function of the Pb film thickness, are shown in figure 3(a). The curves up to 5 ML of Pb increase roughly linearly with the film thickness. At 5 ML, where the structural transition occurs, strong variation of the DR occurs. For energies 0.4 and 0.5 eV the DR increases steeply, whereas for energies higher than 0.7 eV it decreases. For larger thickness all plots, independent of the energy, follow a linear dependence. Two curves, for the highest energies, 2.4 and 2.6 eV, do not show any abrupt changes of the DR within the whole range of the thicknesses.

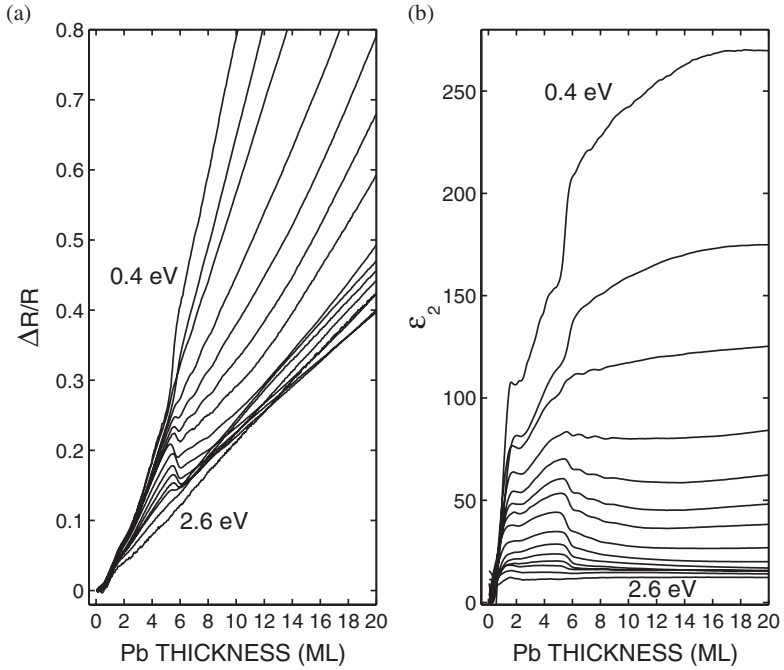

Figure 3. (a) The reflectance difference measured *in situ*, during Pb deposition onto Si(111)-(7×7) substrate at 105 K, for energies, from top to bottom, 0.4, 0.5, 0.6, 0.7, 0.8, 0.9, 1.0, 1.2, 1.4, 1.6, 1.8, 2.0, 2.2, 2.4, and 2.6 eV. (b) The corresponding imaginary part of the dielectric function $\varepsilon_2 = \mathrm{Im}(\varepsilon^{\mathrm{Pb}})$ derived from the experimental data of (a). ε_2 is calculated according to equation (1), for p-polarized light.

3.3. The dielectric function of the growing Pb film

From the data displayed in figure 3(a), using equation (1), the imaginary part of the Pb dielectric constant was calculated. In order to extract the imaginary part of the Pb thin film dielectric function, we assumed that the real part of the dielectric function for the thin Pb film is the same as for bulk Pb [17]. For Pb deposited on Si, owing to the weak sensitivity of the DR, (equation (1)), to the real part of the $\varepsilon^{\mathrm{Pb}}$ variation, this assumption is fully justified. Figure 3(b) shows the imaginary part of the dielectric function, $\mathrm{Im}(\varepsilon^{\mathrm{Pb}})$, versus the film thickness dependence, calculated from the experimental data of figure 3(a).

For these curves a strong thickness dependence is to be noticed. The dielectric function behaves differently for thicknesses below 5 ML than for thicker films. A characteristic feature of the first region is a linear increase of the dielectric function with film thickness. For films thicker than approximately 2 ML the dielectric function also approaches a linear dependence, but with smaller slope than for the thinnest films. The second region begins with an abrupt increase of the dielectric function for the lowest energies and a clear decrease of the dielectric function for the mid energies. For all energies $\mathrm{Im}(\varepsilon^{\mathrm{Pb}})$ saturates for a film thickness of about 15 ML. Due to strong variation of the film crystal structure, each region needs a separate discussion.

3.4. Free electron contribution

The frequency dependent dielectric function may have contributions from several interactions [18]:

$$\varepsilon(\omega) = \varepsilon_\infty + \varepsilon^{\mathrm{f}} + \varepsilon^{i} + \varepsilon^{j}, \tag{3}$$

where ε_∞ denotes ion-core vibrations, ε^{f} is the contribution from the Drude free-carriers, and $\varepsilon^i + \varepsilon^j$ describe inter- and intraband transitions, respectively. Depending on the angular frequency of the propagating light, ω, a particular component of the dielectric function can dominate. In the infrared region the main contribution comes from interaction with free electrons. Neglecting the inter- and intraband contribution, we obtain a Drude-type dielectric function:

$$\varepsilon(\omega) = \varepsilon_\infty - \frac{\omega_{\mathrm{p}}^2}{\omega(\omega + \mathrm{i}\tau^{-1})}, \tag{4}$$

where ω_{p} is the plasma frequency and τ is the electron scattering time. The imaginary part of the dielectric function $\mathrm{Im}\,\varepsilon(\omega) \equiv \varepsilon_2(\omega)$ is then

$$\varepsilon_2(\omega) = \frac{\omega_{\mathrm{p}}}{\omega}\frac{\tau}{\omega^2\tau^2 - 1}. \tag{5}$$

To understand the implication of equation (5), some discussion of the scattering time τ is in order. The equation shows that in the case when $\omega\tau < 1$ the free electron contribution into dielectric function is negative, and it reverses into positive if $\omega\tau > 1$. This situation is met in our studies during growth of the Pb film. It is reasonable to assume that the upper limit for the mean free path length l of electrons is limited by the size of the small Pb grains. Thus for the very thin samples, before the structural transition, as is seen in figure 1(a), it can be as small as 1 or 2 nm. Taking the electron velocity at the Fermi energy $v_{\mathrm{F}} = 1.83$ cm s^{-1} [19] and the mean free path l of the current carriers limited to the grain size, we obtain for $l = 2$ nm the scattering time $\tau = 1.09 \times 10^{-14}$ s. With such a value of the scattering time, $\omega\tau$ is equal to 1 for ω corresponding to the energy of the radiation $\hbar\omega = 0.66$ eV.

This discussion shows that for the thinnest film the imaginary part of the dielectric function of Pb can behave in an unusual way. In fact, for the lowest energies and for thicknesses smaller than 0.6 ML, ε_2 (figure 3(b)) has a negative sign. Therefore, for higher energies, and also for thicknesses larger than about 1 ML, an increase of the scattering time τ should lead to a decrease of ε_2. This is especially true for the lowest energies, when the Drude mechanism dominates. Instead, for 0.4 and 0.5 eV, at the thickness of about 5 ML where the structural transition occurs, the dielectric function steeply increases. We conclude that this is due to the increase of ω_{p}.

The absorption of the radiation can be discussed in terms of optical conductivity. The optical properties of a metal can be described by $\tilde{\varepsilon} = \varepsilon_1 + \mathrm{i}\varepsilon_2$ or, alternatively, by $\tilde{\sigma} = \sigma_1 + \mathrm{i}\sigma_2$. The complex dielectric function and the complex conductivity are related in the following way: $\tilde{\varepsilon} - \varepsilon_\infty = 4\pi\,\mathrm{i}\,\tilde{\sigma}/\omega$. For electrons in partially filled bands, $\tilde{\varepsilon} = 4\pi\,\mathrm{i}\,\tilde{\sigma}/\omega$, a quantity which can be easily calculated from the data presented in figure 3(b). Figure 4(a) shows $\sigma_1 = \omega\varepsilon_2/4\pi$ in units $\Omega^{-1}\mathrm{m}^{-1}$ as a function of the film thickness, for the same energies as in figure 3.

The figure clearly shows structural transition consequences on the optical properties of the ultrathin Pb film. For lower energies (the three upper curves) absorption of the energy increases after transition. As discussed previously, this is caused by the increase of the plasma frequency after the formation of a well ordered crystalline structure. Apparently, the electrons localized within small grains of highly disordered Pb, after transformation into the crystalline phase, begin to contribute much more to the collective excitation through the increase of their density. For higher energies the contribution of the Drude excitations vanishes rapidly as $1/\omega^3$, and for energies larger than about 0.7 eV it plays a minor role.

3.5. The role of the interband optical transitions

For higher energies the optical conductivity shown in the figure 4(a) behaves differently. Here the structural transition manifests as a sudden decrease. To explain this effect we recall the

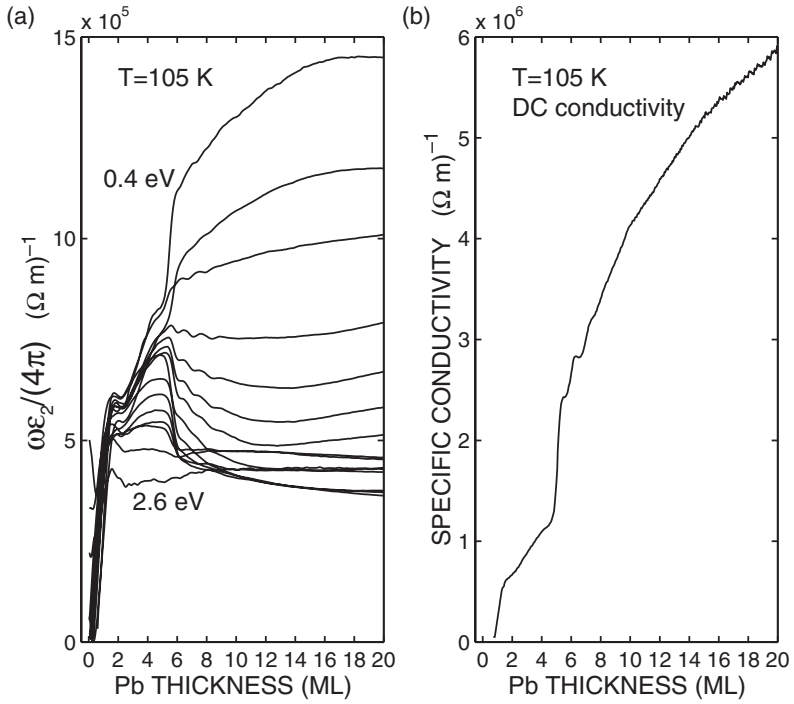

Figure 4. (a) The optical (AC) conductivity of the ultrathin Pb film as a function of the film thickness for several light energies $\hbar\omega$. The quantity is calculated from the data presented in figure 3. (b) The DC electrical conductivity for the ultrathin Pb sample measured during sample deposition. Both AC and DC conductivity are displayed in the same units, Ω^{-1} m^{-1}.

band structure of Pb. It has been shown experimentally [17, 21], and justified by the results of band structure calculations [20], that the onset of the interband transition occurs at light energy of about 1 eV, and at this energy electron states only from a small part of the Pb Brillouin zone are involved in light absorption. It is reasonable to assume that in the disordered film more electrons can be excited between bands than in the ordered phase. This is due to broadening of the energy bands in the amorphous phase. We expect that after the structural transformation, when the band structure of Pb resembles that characteristic of a bulk material and the electron bands are well defined, only a limited number of states is accessible for the optical transition. From the electron band structure calculations it follows that for $\hbar\omega$ from 1 to 1.5 eV optical transitions between filled W_6 and empty W_7 bands [17, 20] are possible.

3.6. Comparison with DC conductivity data

The AC conductivity can be compared with the DC conductivity which was measured during the film deposition in the same conditions as during the optical studies. Figure 4(b) shows an example of the DC conductivity. The similarity with optical conductivity, especially with the curve for 0.4 eV in figure 4(a), is striking. The DC conductivity follows the same thickness dependence as AC. The structural transition manifests as a sudden increase of the conductivity at the same thickness as for the AC curve. This result clearly shows that for energies lower than about 0.6 eV only Drude excitations define the optical properties of the Pb film. Interestingly, after the structural transition both AC and DC conductivities show the same oscillations with

a periodicity equal to 1 ML of Pb. Its appearance is related to the periodic variation of the scattering rate of the current carriers as a consequence of the perfect layer-by-layer growth of the ultrathin film [4].

4. Conclusion

Ultrathin Pb films grown on Si(111)-(7 × 7) substrates at 105 K have been shown to be particularly suited to characterization by the differential reflectivity method. STM and RHEED studies have shown that the Pb film up to the critical thickness of about 5 ML forms an amorphous layer. After the structural transition it grows in a layer-by-layer mode and has a well ordered crystalline structure. All stages of the film growth and the morphological changes are reflected in the variation of the imaginary part of the dielectric function of Pb. Extended measurements in the broad energy range of the radiation allowed us to distinguish free-electron (Drude) excitations from interband transitions.

We have found that at radiation energies from 0.4 to 0.6 eV the transition manifests as an increase of ε_2, and this phenomenon is explained by an increase of the free-electron plasma frequency caused by electron delocalization and not by the increase of the scattering time. At higher energies, when the interband excitations dominate, the structural transition manifests through a decrease of ε_2. This behaviour is explained as a consequence of the creation of a well defined band structure of the crystalline Pb.

The comparison between AC and DC conductivities made in this study clearly shows that the optical method can be used for studying the electrical conductivity properties of ultrathin films and overlayers. This finding is important for the study of the galvanomagnetic properties of metallic quantum wells hardly accessible for any conventional method requiring electric contacts [3, 4]. The results of this study may help to understand weak-localization and insulator-to-metal transition phenomena in ultrathin metallic films.

References

[1] Botsma T I M and Hibma T 1993 *Surf. Sci.* **287/288** 921
[2] Edwards K A, Howes P B, Macdonald J E, Hibma T, Bootsma T and James M A 1996 *Physica* B **221** 201
[3] Jałochowski M and Bauer E 1988 *Phys. Rev.* B **38** 5272
[4] Jałochowski M, Hoffmann M and Bauer E 1995 *Phys. Rev.* B **51** 7231
[5] Jałochowski M, Knoppe H, Lilienkamp G and Bauer E 1992 *Phys. Rev.* B **46** 4693
[6] Jałochowski M, Hoffmann M and Bauer E 1996 *Phys. Rev. Lett.* **76** 4227
[7] Vilfan I, Henzler M, Pfennigstorf O and Pfnür H 2002 *Phys. Rev.* B **66** 241306
[8] Edwards K A, Howes P B, Macdonald J E, Hibma T, Bootsma T and James M A 1999 *Surf. Sci.* **424** 169
[9] Henning P F, Homes C C, Maslow S, Carr G L, Basov D N, Nikolić B and Strongin M 1999 *Phys. Rev. Lett.* **83** 4880
[10] Tu J J, Homes C C and Strongin M 2003 *Phys. Rev. Lett.* **90** 017402
[11] McIntyre J D E and Aspnes D E 1971 *Surf. Sci.* **24** 417
[12] Borensztein Y, Alameh R and Roy M 1994 *Phys. Rev.* B **50** 1973
[13] Borensztein Y and Alameh R 1992 *Surf. Sci. Lett.* **274** L509
[14] Hingerl K, Aspnes D E and Kamiya I 1993 *Surf. Sci.* **287/288** 686
[15] McGilp J F 2001 *Phys. Status Solidi* a **188** 1361
[16] Jałochowski M, Strożak M and Zdyb R 2002 *Phys. Rev.* B **66** 205417
[17] Liljenvall H G, Mathewson A G and Myers H P 1979 *Phil. Mag.* **22** 243
[18] Huang W C and Lue J T 1994 *Phys. Rev.* B **49** 17279
[19] Ashcroft N W and Mermin N D 1976 *Solid State Physics* (Fort Worth: Saunders College Publishing)
[20] Anderson J R and Gold A V 1965 *Phys. Rev.* **139** A1459
[21] Mathewson A G, Myers H P and Nillson P O 1973 *Phys. Status Solidi* b **57** K31